ION TEMPERATURE MEASUREMENT BY NEUTRAL ENERGY ANALYZER IN HIGH-FIELD TOKAMAK

Nakamura, Kazuo
Research Institute for Applied Mechanics, Kyushu University : Research Associate

Hiraki, Naoji
Research Institute for Applied Mechanics, Kyushu University : Research Associate

Toi, Kazuo
Research Institute for Applied Mechanics, Kyushu University : Associate Professor

Itoh, Satoshi
Research Institute for Applied Mechanics, Kyushu University : Professor

https://doi.org/10.5109/6771951

出版情報：Reports of Research Institute for Applied Mechanics. 27 (86), pp.125-146, 1979-12.
九州大学応用力学研究所
バージョン：

Reports of Research Institute for Applied Mechanics
Vol. XXVII, No. 86, 1980

ION TEMPERATURE MEASUREMENT BY NEUTRAL ENERGY ANALYZER IN HIGH-FIELD TOKAMAK TRIAM-1

Kazuo NAKAMURA*, Naoji HIRAKI*,
Kazuo TOI** and Satoshi ITOH***

The measurement of the ion temperature of the TRIAM-1 tokamak plasma is carried out by using a seven-channel neutral energy analyzer. The temporal and spatial variations of the ion temperature have been obtained with the spatial resolution of ± 4.3 mm and the temporal resolution of 100 μsec. The energy range of the analyzed neutral particles is from 0.2 to 8 keV.

The energy spectrum in the TRIAM-1 plasma without the strong gas puffing usually consists of two-component Maxwellian; the one represents the thermal part which is a superposition of the contribution from a hot region ($T_i=100-300$ eV) and that from an edge region ($T_i \approx 50$ eV), and the other represents the superthermal part ($T_i \approx 1$ keV). The neutral particle energy spectra at several vertical positions are obtained by scanning the analyzer in the vertical direction. From those spectra, the radial profile of the ion temperature is derived by means of the nonlinear optimization method.

Key words: Neutral energy analyzer, high-field tokamak TRIAM-1, radial profile, trapped particles, reflection by the wall

1. Introduction

The high-field tokamak device TRIAM-1 (The 1st Tokamak of Research Institute for Applied Mechanics)[1] was constructed to investigate the confinement of the high-density plasma and the turbulent heating: the major radius $R=25.4$ cm, the minor radius of molybdenum limiter $a_L=4$ cm and the maximum toroidal field $B_T=40$ kG. The experiment in

* Research Associate, Research Institute for Applied Mechanics, Kyushu University.
** Associate Professor, Research Institute for Applied Mechanics, Kyushu University.
*** Professor, Research Institute for Applied Mechanics, Kyushu University.

TRIAM-1 has been started since the end of 1978. The maximum values of the principal plasma parameters obtained by ohmic heating alone are as follows; central electron temperature $T_{e0}=640\,\mathrm{eV}$, central ion temperature $T_{i0}=280\,\mathrm{eV}$ and line-average electron density $\bar{n}_e=2.2\times10^{14}\mathrm{cm}^{-3}$. The turbulent heating has been carried out by applying the high electric field to the typical tokamak discharge in the toroidal direction, and the efficient ion heating has been observed.

A seven-channel neutral energy analyzer was constructed for the ion temperature measurement of the TRIAM-1 tokamak plasma. In this report the design of the neutral energy analyzer and the results of the ion temperature measurements are described. The radial profile of the ion temperature has been derived by the nonlinear optimization method from the energy spectra obtained by scanning the analyzer in the vertical direction.

2. The neutral energy analyzer

2.1 Ion temperature measurement by neutral energy analyzer

A hot hydrogen ion ($\underline{H}^+$) in a plasma is converted to an energetic neutral particle ($\underline{H}$) through the charge-exchange process with a cold neutral particle (H),

$$\underline{H}^+ + H \rightarrow \underline{H} + H^+ . \tag{1}$$

The energetic neutral particle emitted from the plasma by the above process enters the neutral energy analyzer and is re-ionized by the hydrogen gas in the stripping cell as

$$\underline{H} + H_2 \rightarrow \underline{H}^+ + H_2 + e^- . \tag{2}$$

These ions are analyzed electrostatically or magnetically as shown in Fig. 1. For electrostatic deflection the energy of the ion is proportional to the applied voltage (*"energy analysis"*), and for magnetic deflection the momentum is proportional to the magnetic field (*"momentum analysis"*). In order to obtain the energy spectrum of neutral particles during one shot of discharge, the sawtooth voltage should be applied to the analyzer electrodes in case (a) of Fig. 1, since this type is single channel detection. Since the several detectors can be used in cases (b) and (c), the applied voltage or magnetic field is maintained stationary. By using both deflection methods in cascade it is possible to determine the charge-to-mass ratio. Since the duration time of the TRIAM-1 discharge is not so long ($\approx$10 msec), we adopted the electrostatic deflection method (b) where several detectors can be used simultaneously. The deflection methods adopted in tokamaks are listed up in Table 1.

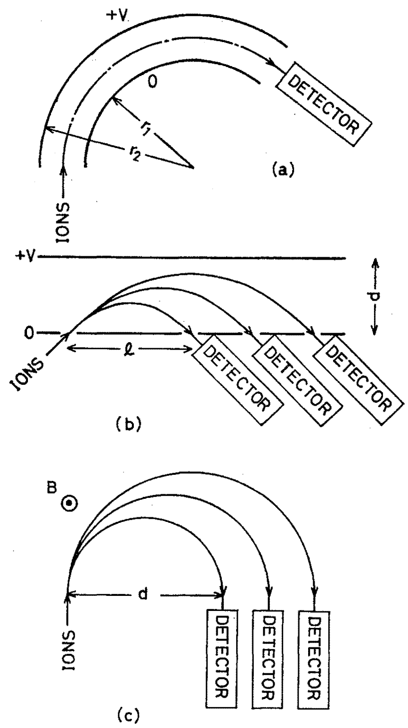

Fig. 1 Schematic diagram of the methods of deflection in energy analyzer.

(a) electrostatic deflection (energy analysis)

$$E \equiv \frac{1}{2} mv^2 = \left(\frac{e}{2\ln(r_2/r_1)}\right) V$$

(b) electrostatic deflection (energy analysis)

$$E \equiv \frac{1}{2} mv^2 = \left(\frac{el}{2d}\right) V$$

(c) magnetic deflection (momentum analysis)

$$p \equiv mv = \left(\frac{ed}{2}\right) B$$

We briefly describe the procedure for determining the ion temperature by the neutral energy analysis. The number of ions counted by the detector N is expressed as

$$N = n_0 \sigma_{10} v_i f(E) \Delta V \frac{\Delta\Omega}{4\pi} \Delta E \Delta t \eta \zeta \,, \tag{3}$$

where n_0: neutral particle density in plasma,

σ_{10}: charge-exchange cross-section of $\underline{H}^+$ with H,

Table 1. Neutral energy analyzers in tokamaks

Method of deflection	Tokamaks adopting the method
Electrostatic deflection shown in Fig. 1(a)	ALCATOR[2], ATC[3], TFR[4], TTT[5]
Electrostatic deflection shown in Fig. 1(b)	DITE[6], JFT-2[7], JIPP T-II[8], ORMAK[9], PLT[10], TRIAM-1
Magnetic deflection shown in Fig. 1(c)	
Electrostatic and magnetic deflection	PDX[11], PLT[12], PULSATOR[13], T-4[14], T-10[15),16]

v_i: ion velocity,
$f(E)$: ion energy distribution function,
ΔV: the volume viewed by the analyzer,
$\Delta\Omega$: the solid angle viewing the analyzer,
ΔE: the energy resolution,
Δt: the time interval during which the pulses are counted,
η: conversion factor of the stripping cell,
ζ: the relative efficiency of each channel.

If the energy distribution of plasma ions is Maxwellian, the distribution function is expressed as

$$f(E) = n_i \frac{2}{\sqrt{\pi}} \frac{E^{1/2}}{T_i^{3/2}} e^{-E/T_i}. \tag{4}$$

Since the energy resolution ΔE is proportional to the applied voltage V,

$$\Delta E = CV, \tag{5}$$

where the coefficient C depends on the geometrical factor of the analyzer and $C=92.3\,\mathrm{eV/kV}$ in TRIAM-1. From eqs. (3)-(5), the following quantity F can be related with the ion energy distribution function as

$$F \equiv \frac{N}{\eta E V \sigma_{10} \zeta} = K \frac{n_0 n_i}{T_i^{3/2}} e^{-E/T_i}, \tag{6}$$

where $K = \sqrt{\frac{2}{M}} \frac{2}{\sqrt{\pi}} \Delta V \frac{\Delta\Omega}{4\pi} C \Delta t = \text{const.}$, (7)

and M is the mass of ion species. We can estimate the ion temperature from the slope of the semi-logarithmic plot of F with respect to the energy E.

2.2 The neutral energy analyzer in the TRIAM-1 tokamak

Figure 2 shows the schematic view of the neutral energy analyzer

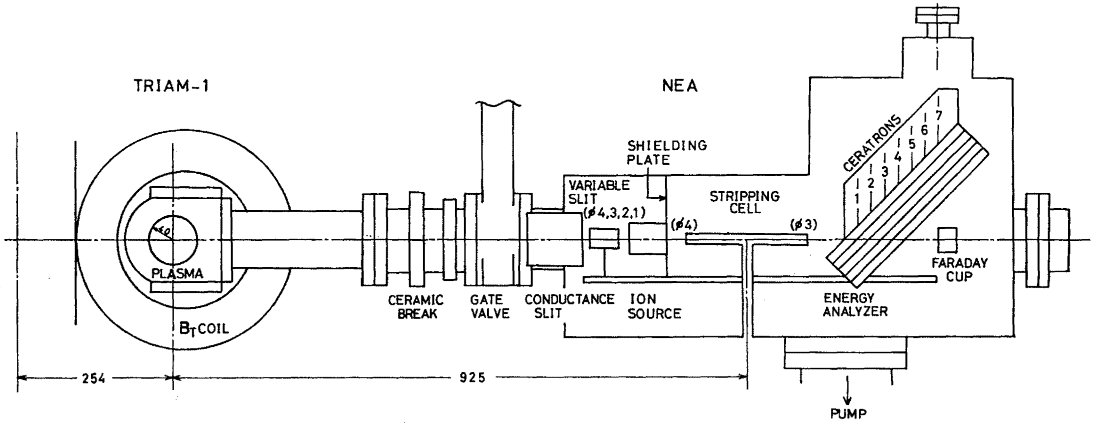

Fig. 2 Cross-sectional view of neutral energy analyzer (NEA) in TRIAM-1.

(NEA) in TRIAM-1. The variable slit, ion source, stripping cell, energy analyzer and ceratrons are equipped on the same base. The base can be moved vertically to measure the radial profile of the ion temperature. The ceramic break insulates NEA from the vacuum chamber of TRIAM-1 device. The gate valve is opened for only 5 sec before and after the tokamak discharge to prevent the residual gas in NEA from flowing into TRIAM-1. The conductance slit is equipped to reduce the conductance between torus and analyzer chamber and collimate the plasma area viewed by the analyzer. The conductance slit has 9 square holes of 4×4 mm-cross-section and 90 mm-length to measure the vertical profile of the energy spectra of the neutral particles. Although the toroidal chamber is filled with hydrogen of 6.4×10^{-4} Torr, the analyzer chamber can be evacuated differentially up to 2×10^{-5} Torr by using the pumping system with a moderate pumping speed. The chamber is made of the stainless steel (SUS 304) of 6 mm thick and the field penetration time is 31.9 μsec. The diameters of the variable slit are 4, 3, 2 and 1 mm, and the spatial resolutions are ±6.4, ±6.4, ±5.7 and ±4.3 mm at the plasma, respectively. The length of the stripping cell is 20 cm, and the diameters of the entrance and the exit slits are 4 mm and 3 mm, respectively. In this experimental series, the cell is filled with hydrogen gas to 4×10^{-4} Torr. The parallel plates of the energy analyzer can be imposed up to 5 kV. The relation between the applied voltage V and the energy of the channel E_i is listed in Table 2. The stray magnetic field is less than 2 G at position of the energy analyzer (Appendix A).

Table 2. Relation of the energy of the i-th channel E_i and the applied voltage between the parallel plates in the energy analyzer V.

V (kV)	(keV)						
	E_1	E_2	E_3	E_4	E_5	E_6	E_7
0.4178	0.1	0.2	0.3	0.4	0.5	0.6	0.7
0.8357	0.2	0.4	0.6	0.8	1.0	1.2	1.4
1.2535	0.3	0.6	0.9	1.2	1.5	1.8	2.1
1.6713	0.4	0.8	1.2	1.6	2.0	2.4	2.8
2.0892	0.5	1.0	1.5	2.0	2.5	3.0	3.5
2.5070	0.6	1.2	1.8	2.4	3.0	3.6	4.2
2.9248	0.7	1.4	2.1	2.8	3.5	4.2	4.9
3.3427	0.8	1.6	2.4	3.2	4.0	4.8	5.6
3.7605	0.9	1.8	2.7	3.6	4.5	5.4	6.3
4.1784	1.0	2.0	3.0	4.0	5.0	6.0	7.0
4.5962	1.1	2.2	3.3	4.4	5.5	6.6	7.7
5.0140	1.2	2.4	3.6	4.8	6.0	7.2	8.4

The seven ceratrons (EMS-6081 B of MURATA MFG. CO., LTD.) are used as the ion detectors. The shielding plate prevents the neutral flux coming through the upper holes of the conductance slit from entering the ceratrons directly. The chamber is evacuated by a turbo molecular pump with a pumping speed of 450 l/sec for nitrogen. The base pressure is 2×10^{-6} Torr.

The electronic circuit assembly for counting the pulses from ceratrons is shown in Fig. 3. The load resistance of ceratron R is 1 kΩ. The high voltage $V_{HG}=3$ kV is applied to the entrance of the ceratron, and $V_{TG}=100$ V to the collector plate. The height of the output pulse of the ceratrons is about 50 mV and the rise time is 0.2 μsec. The gain of the pre-amp is 10 and that of the linear amp is 2. Therefore the pulses are amplified to about 1 V. The discriminater suppresses the pulses lower than 80 mV. The maximum counting rate of this system is 10 MHz. The gate pulse generator produces a gate pulse every 100 μsec. The pulse-count by the multichannel scaler is displayed on the cathode ray tube and output to the digital printer.

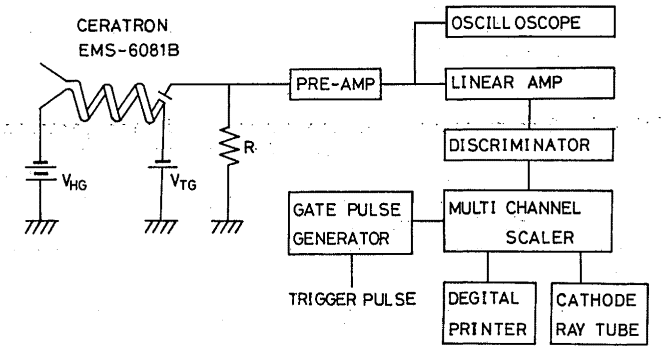

Fig. 3 Electronic circuit assembly for counting the pulses from ceratrons in the neutral energy analyzer.

2.3 Calibration of the neutral energy analyzer

The parameter N in eq. (6) is obtained from the above mentioned procedure, and E and V in eq (6) are given beforehand. The variables σ_{10}, η and ζ are determined by the calibration experiment. However, the preparation for calibration is not finished. Therefore, we use the plausible data. We use the data of Hasted[17] as the charge-exchange cross-section σ_{10}. The conversion factor η shown in Fig. B-1 has been quoted from the data of DITE[12] on assumption that η is proportional to pl (p is the filling pressure of the stripping cell and l is the length of the cell) (Appendix B). The relative efficiency ζ is experimentally deduced from the ratio of the neutral fluxes which enter each ceratron.

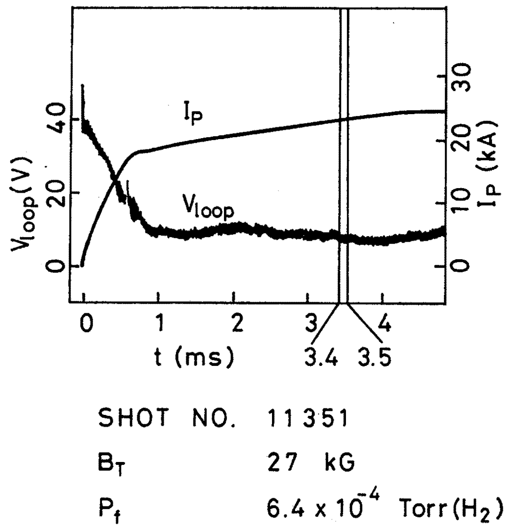

Fig. 4 Waveform of the tokamak discharge produced for determining the relative efficiency of the multichannel detectors. I_p and V_{loop} are the plasma current and loop voltage, respectively.

Table 3. The measured relative efficiency of each ceratron. The relative efficiencies of the 6th and 7th channels are not used to obtain the ion energy spectra, since the values are remarkably smaller than that of the 1st channel.

Channel No.	1	2	3	4	5	6	7
ζ	1	1.59	3.67	14.0	7.81	…	…

As the neutral particle source, we adopt the TRIAM-1 discharge of the waveform shown in Fig. 4. The neutral particles are counted during 100 μsec from 3.4 to 3.5 msec. The function G in Fig. 5 has been obtained as a function of the particle energy E by varying V on shot-to-shot. It should be noted that the fitting curve of each channel has the similar form, i. e. they coincide each other if they are shifted vertically. From this fact, ζ is independent of the particle energy E in the range of 0.2 keV to 3.6 keV. The relative efficiency ζ is obtained from the ratio of the value G in the same energy (Table 3).

Using these ζ-values, we can express the curves in Fig. 5 by the single fitting curve as in Fig. 6. This spectrum can be expressed by two component Maxwellian of the temperature 140 eV and 810 eV. The former represents the ion temperature of the bulk ion (T_i(bulk)) and

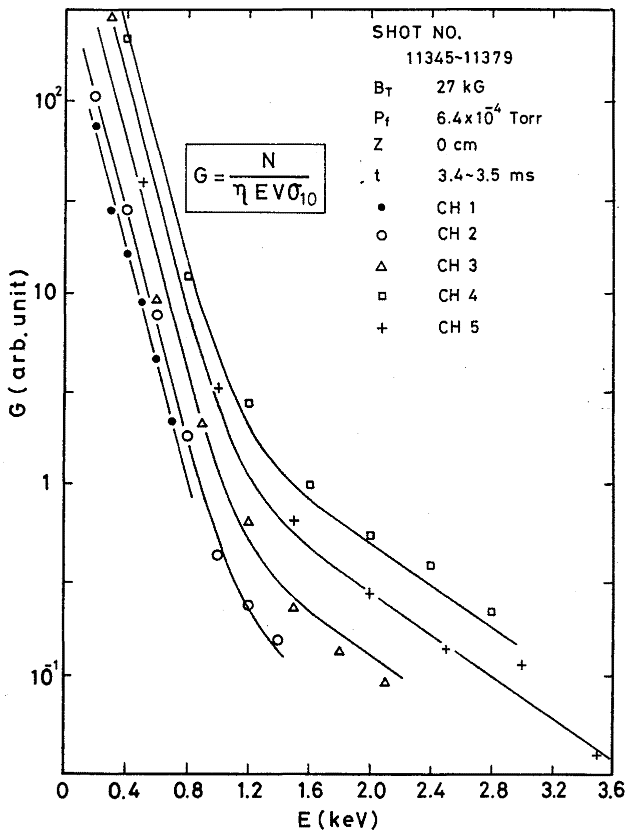

Fig. 5 The energy spectra obtained by each channel without the correction of the relative efficiency.

the latter the tail (T_i(tail)). That is consistent with the following three facts:

(1) This bulk ion temperature agrees well with the value predicted by the Artsimovich scaling law[18] as shown by the symbol (◎) in Fig. 7,

(2) the ratio of the $n_0 n_i/T_i^{3/2}$-value of the tail to that of the bulk ion is very small to be 1.48×10^{-3}, and

(3) the electron temperature of this plasma is 260 eV and the ratio to the ion temperature of the bulk ions is 1.9.

3. Measurement of the radial profile of the ion temperature

3.1 Systematic determination of the ion temperature from the energy spectra

In the subsection 2.3 we obtained the ion temperature from the

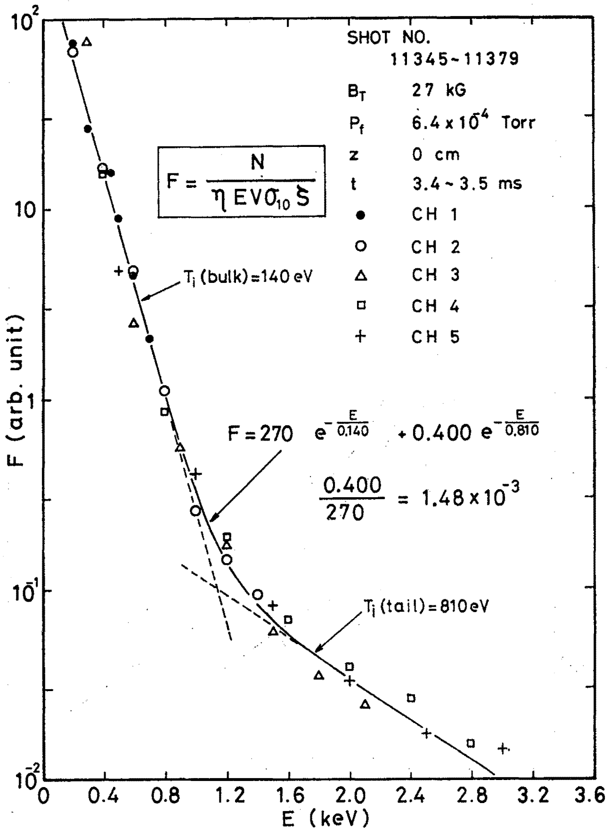

Fig. 6 The energy spectrum re-arranged from Fig. 5 by the correction of the relative efficiency of the detectors.

slope of the energy spectrum where the fitting curve was drawn properly by hand. Here in order to process the data systematically, we propose the following numerical method: The fitting curve is easily obtained by the nonlinear optimization method[19] so that the following objective function D should be minimized with respect to six parameters (A_1, A_2, A_3, T_1, T_2 and T_3) on two constraining conditions,

$$D = \sum_j \left[A_1 e^{-E_j/T_1} + A_2 e^{-E_j/T_2} + A_3 e^{-E_j/T_3} - F(E_j)\right]^2, \tag{8}$$

$$A_1 \geqq A_2 \geqq A_3 \geqq 0\,, \tag{9}$$

$$0 \leqq T_1 \leqq T_2 \leqq T_3\,, \tag{10}$$

where the simplex method[20] is used as the minimizing code. The temperature T_3 represents the temperature of the superthermal ions. The spectrum excluding the superthermal part measured at the height

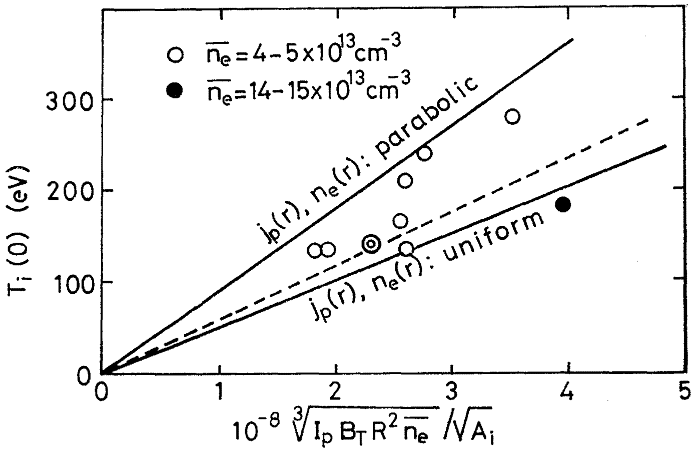

Fig. 7 Comparison of the central ion temperatures obtained in TRIAM-1 with the Artsimovich scaling. The ion temperature from Fig. 6 (T_i(bulk)) is indicated by the symbol (◎).

$z(A_1 e^{-E_l/T_1}+A_2 e^{-E_l/T_2})$ has the information concerning the thermal ions in the region $z \leq r \leq a_L$. The temperatures T_1 and T_2 approximately represent the ion temperature near the region $r \approx a_L$ and $r \approx z$, respectively. The correctness of this approximation is discussed in the next subsection.

Figure 8(a)-(e) shows the spectra measured below the torus midplane during 100 μsec from 2.5 to 2.6 msec in the discharge in Fig. 4. The fitting curves have been derived by the above method. The error of the bulk ion temperature has been estimated by the procedure described in Appendix C. The ion temperature of the bulk plasma are plotted in Fig. 9 together with the results measured above the torus midplane. The asymmetry with respect to the torus midplane may be explained by the effect of the trapped ions[21),22)], taken into account that ions drift upwardly due to the curvature of toroidal field. Moreover, it should be noted that $T_i(z=-4\,\text{cm})=0.6\times T_i(z=0\,\text{cm})$. This fact is considered to be due to the effect of the reflection of fast neutral particles by the wall[23)].

3.2 Calculation of the ion temperature profile

In the previous section the vertical profile of "*ion temperature*" $T_i(z)$ has been obtained by plotting the temperature T_2 in eq. (8) at the corresponding height z. In this section the radial profile $T_i(r)$ is derived from the all spectra shown in Figs. 8(a)-(e) using the following model, where the superthermal part is rejected from the spectra.

The calculation model is as follows: The profiles of the electron

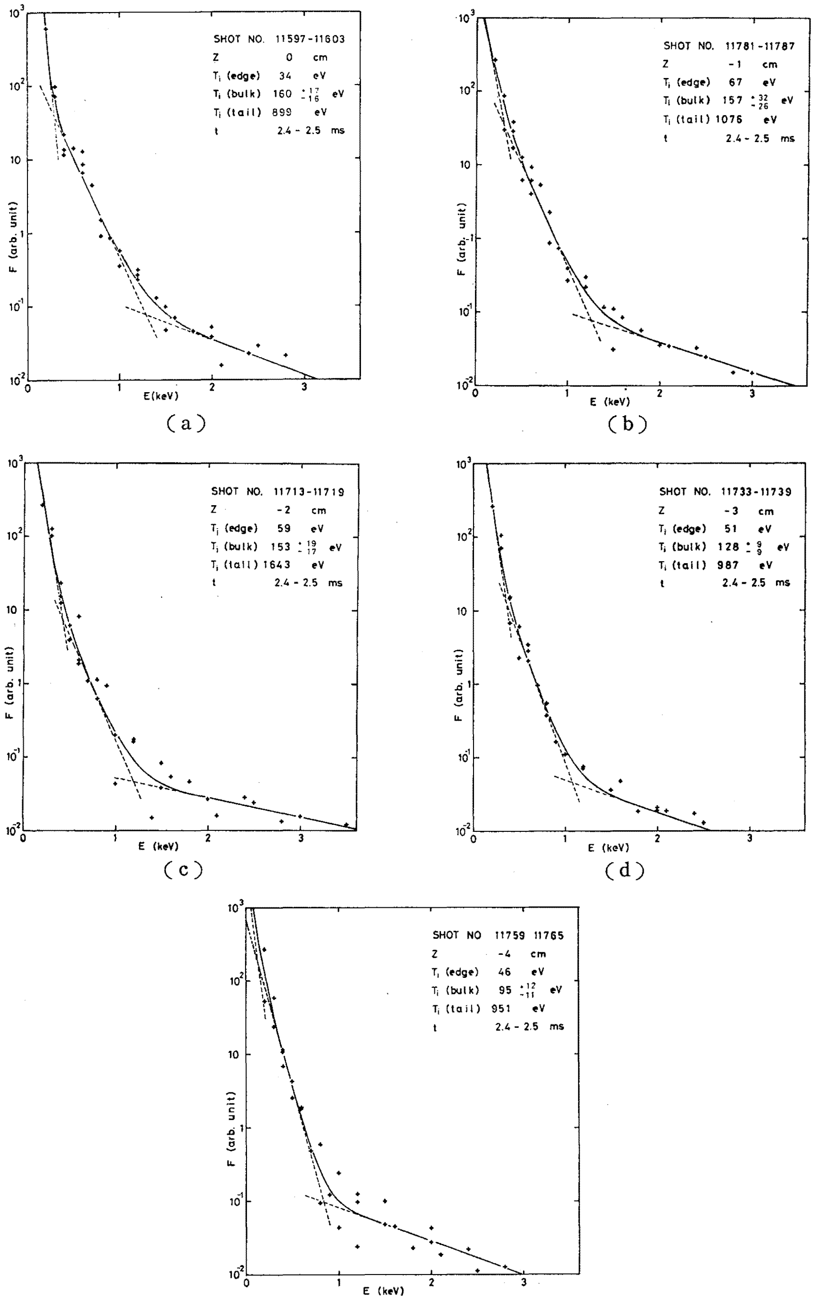

(a) (b) (c) (d) (e)

Fig. 8 The neutral energy spectra measured at the height (a) $z=0$, (b) $z=-1$, (c) $z=-2$, (d) $z=-3$ and (e) $z=-4$ cm.

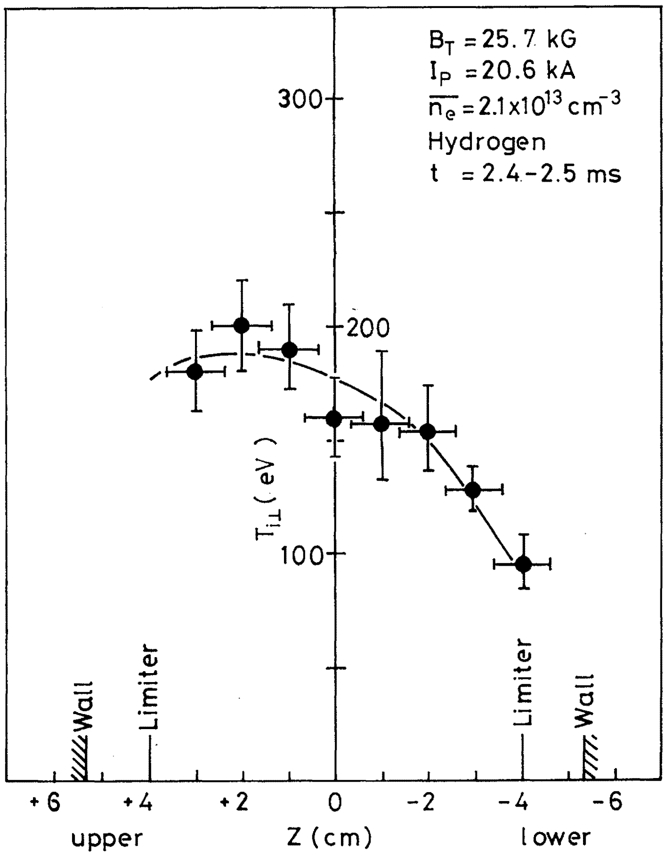

Fig. 9 The vertical profile of the bulk ion temperature derived from the energy spectra shown in Figs. 8(a)—(e) and those in the upper region of plasma.

density $n_e(r)$ and the electron temperature $T_e(r)$ are assumed as

$$n_e(r) = n_e(0)\{0.8(1-x^2)+0.2\}\ , \tag{11}$$

$$T_e(r) = T_e(0)\{0.8(1-x^2)+0.2\}\ , \tag{12}$$

$$x = r/a\ , \tag{13}$$

$$a = 4\,\text{cm (limiter radius)}\ , \tag{14}$$

$$n_e(0) = 1.36\,\bar{n}_e\ , \tag{15}$$

where the experimental data are used for $\bar{n}_e = 2.1\times10^{13}\text{cm}^{-3}$ and $T_e(0) = 260\,\text{eV}$.

The ion temperature profile is assumed by using the unknown parameters $T_i(0)$, t_1 and t_2,

$$T_i(r) = T_i(0)\{(1-t_1)(1-x^2)^{t_2}+t_1\} . \tag{16}$$

From eqs. (11)-(16), the neutral density profile is calculated by the following equation

$$\frac{n_0(r)}{n_0(a)} = \exp\left\{-\frac{1}{v_0}\int_r^a (n_e\langle\sigma v\rangle_I + n_i\langle\sigma v\rangle_{cx})\mathrm{d}r\right\} , \tag{17}$$

where the mono-energetic cold neutrals with $v_0 = 3\,\mathrm{eV}$ are assumed to enter the plasma from the wall and to be attenuated by the ionization or charge-exchange. The rates of the ionization $\langle\sigma v\rangle_I$ and the charge-exchange $\langle\sigma v\rangle_{cx}$ have been represented by the following relations[24) :

$$\log_{10}\langle\sigma v\rangle_I = -0.5151\,x - 2.563/x - 5.231 \tag{18}$$

$$x = \log_{10} T_e(\mathrm{eV}) \tag{19}$$

$$\langle\sigma v\rangle_{cx} = \sigma_{cx} v_{rel} \tag{20}$$

$$\sigma_{cx} = \left[7.6\times10^{-8} - 1.06\times10^{-8}\times\log_{10}\left(\frac{1}{2}m\,v^2_{rel}(\mathrm{eV})\right)\right]^2 \ \mathrm{cm}^2 \tag{21}$$

$$v_{rel} = \left[\frac{8}{\pi}\left(\frac{T_i}{m_i}\right)\right]^{1/2} \tag{22}$$

It is assumed that the ion density profile $n_i(r)$ is similar to that of electron density and $n_i(0) = n_e(0)$.

If $n_0(r)$, $n_i(r)$ and $T_i(r)$ are given, the neutral particle flux F can be estimated on the same geometry in the experiment (Fig. 10),

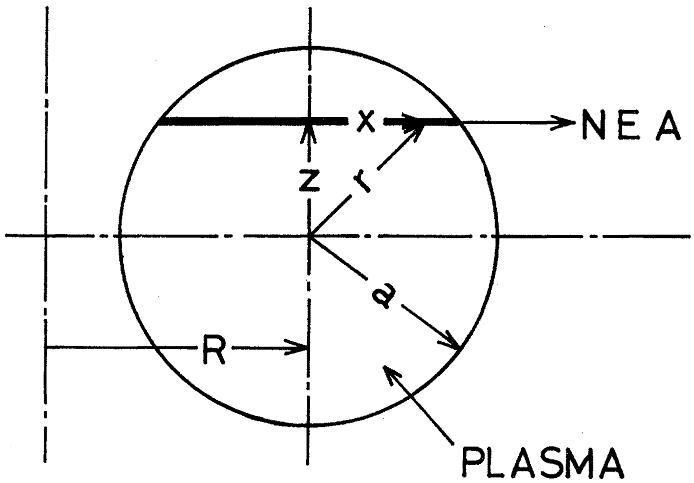

Fig. 10 The schematic diagram of the viewing plasma area of the energy analyzer.

$$F_{\mathrm{cal}}(z,\,E) = \int_0^{\sqrt{a^2-z^2}} F\mathrm{d}x = K\int_0^{\sqrt{a^2-z^2}} \frac{n_0(r)\,n_{\mathrm{i}}(r)}{T_{\mathrm{i}}(r)^{3/2}}\,\mathrm{e}^{-E/T_{\mathrm{i}}(r)}\,\mathrm{d}x \tag{23}$$

where the impermeability of the plasma for the fast neutral particles is negligible because of low electron density[25]. We determine the unknown parameters $T_{\mathrm{i}}(0)$, t_1 and t_2 so that the following objective function Φ is minimized with respect to those parameters,

$$\Phi(T_{\mathrm{i}}(0),\,t_1,t_2) = \sum_{\mathrm{i}}\sum_{\mathrm{j}}\,[F_{\mathrm{cal}}(z_{\mathrm{i}},\,E_{\mathrm{j}}) - F(z_{\mathrm{i}},\,E_{\mathrm{j}})]^2\,, \tag{24}$$

where $F(z_{\mathrm{i}}, E_{\mathrm{j}})$ is the quantity measured at the height z_{i}. The simplex method[20] is used also here.

Figure 11 shows the profile obtained by the above calculation. The central ion temperature (173 eV) derived from the above calculation is 8 % higher than the measured central ion temperature (160 eV). That is due to the effect of the nonuniform distribution of the neutral density, the ion density and the ion temperature. The difference between $T_{\mathrm{i}}(z)$ obtained directly by the neutral energy analyzer and $T_{\mathrm{i}}(r)$ derived from the above calculation is within 10 % in case of low electron density $n_{\mathrm{e}} \approx 2\times10^{13}\mathrm{cm}^{-3}$. In the high density plasma, the above impermeability of plasma considerably affects the determination of the ion temperature and the profile. The true radial prfile of ion temperature will be derived from the above analysis that takes into account of the impermeability of plasma for the neutral particles and the reflection of the fast neutral particles by a wall.

4. Conclusion

The seven-channel neutral energy analyzer has been constructed and the measurement of the ion temperature profile is possible with the spatial resolution of ± 4.3 mm at the plasma and the temporal resolution 100 μsec.

The energy spectra can be divided into the three parts, each of which represents the bulk ions in the plasma edge, the bulk ions in the central hot plasma, and the superthermal ions. The ion temperature profile exhibits the asymmetry with respect to the torus midplane, which may be due to the effect of the trapped ions. The radial profile of the ion temperature has been calculated from the spectra obtained at the height $z=0$, -1, -2, -3 and -4 cm by using the nonlinear optimization method. As a result the calculated central ion temperature (173 eV) is 8 % higher than the bulk ion temperature (160 eV) determined from the spectrum measured at $z=0$ cm in case of the line-average electron density $\bar{n}_{\mathrm{e}}=2.1\times10^{13}\mathrm{cm}^{-3}$. The above difference of the ion temperatures is due to the effect of the nonuniform profiles of plasma parameters.

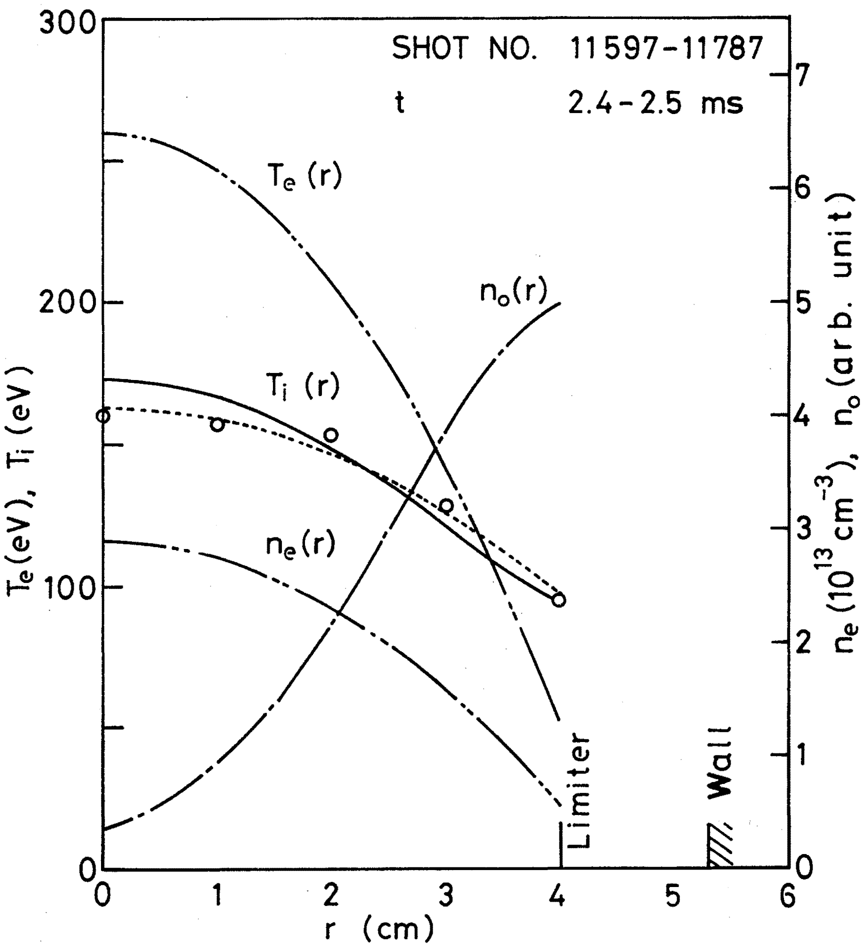

Fig. 11 The radial profile of the ion temperature (——) calculated from the spectra shown in Figs. 8(a)—(e) by the nonlinear optimization method. The open circles indicate the bulk ion temperatures ($z \leqq 0$ cm) shown in Fig. 9 and the broken line (······) is the fitting curve.

The ion temperature measured at the limiter ($z = -4$ cm) is unexpectedly high as the 60 % value of the central ion temperature. That is considered to be due to the effect of the reflection by the wall.

Acknowledgement

The authors would like to express their gratitude to Professor N.

Yajima and Professor K. Kitajima for their continunus encouragements, and to Mr. S. Kawasaki and Mr. H. Nakashima for the technical assistance in the experiment. The authors also would like to express gratitude to Dr. K. Kadota, Dr. N. Noda and Dr. Y. Kawasumi for their offering of the useful information concerning the design of the neutral energy analyzer in the JIPP T-II tokamak.

The analysis of the neutral energy analyzer data was made on MELCOM COSMO 900 computer system at Research Institute for Applied Mechanics.

References

1) Hiraki, N., Itoh, S., Kawai, Y., Toi, K., Nakamura, K. and Mitarai, O.: *Confinement of Ohmically Heated Plasmas and Turbulent Heating in High-Magnetic-Field Tokamak TRIAM-1*, Reports of Research Institute for Applied Mechanics **27** No. 85 (1979) 85.

2) Gaudreau, M. P. J., Kislyakov, A. I. and Sokolov, Yu. A.: *Investigation of Fast-Atom Fluxes in the High-Density Plasma in Alcator*, Nuclear Fusion **18** No. 12 (1978) 1725.

3) Goldston, R. J.: *Charge-Exchange Measurements of the Radial Profiles of Parallel and-Anti-Parallel Ion Energy Distribution on ATC*, Nuclear Fusion **18** No. 12 (1978) 1611.

4) Equipe TFR: *Ion Temperature in the TFR Tokamak*, Nuclear Fusion **16** No. 2 (1976) 279.

5) Nakagawa, Y. and Medley, S. S.: *On the Temporal and Spatial Evolution of Energetic Ion Production in the Texas Turbulent Torus*, J. Phys. Soc. Japan **43** No. 4 (1977) 1385.

6) Summers, D. D. R., Gill, R. D. and Stott, P. E.: *A Neutral Particle Analyzer for Plasma Diagnostics*, CLM-P 514 (1978).

7) Takeuchi, H., Takahashi, K., Shirakata, H. and Funahashi, A.: Report of Japan Atomic Energy Research Institute, JAERI-M 6048 (1975).

8) Kawasumi, Y., Kadota, K. Noda, N. and Fujita, J.: *Ion Temperature Measurement with Neutral Particle Energy Analyzer*, Anual Review of Institute of Plasma Physics (April 1977–March 1978) 18.

9) Barnett, C. F. and Ray, J. A.: *A Calibrated Neutral Atom Spectrometer for Measuring Plasma Ion Temperatures in the* 0.165- *to* 10-*keV Energy Region*, Nuclear Fusion **12** (1972) 65.

10) Equip TFR: *Tokamak Plasma Diagnostics*, Nuclear Fusion **18** No. 5 (1978) 647.

11) Kaita, R., Davis, S. L. and Medley, S. S.: *Monte Carlo Simulation of Ion Trajectories in the Modified PDX Thermal Charge Exchange Analyzer*, PPPL-1493 (1978).

12) Davis, S. L., Medley, S. S. and Brusati, M.: *The Charge Exchange Analyzer for Mass Resolved Ion Temperature Measurements on PLT*, PPPL-1478 (1978).

13) Wharton, Charles B.: *A Review of Energetic Neutral Particle Plasma Diagnostics*, Proc. the Course on Plasma Diagnostics and Data Acquisition (Varrenna, Italy 1978) 70.

14) Afrosimov, V. V., Berezovskii, E. L., Gladkovskii, I. P., Kislyakov, A. I., Petrov, M. P. and Sadovnikov, V. A.: *Multichannel Energy and Mass Analyzer for Atomic Particles*, Sov. Phys. Tech. Phys. **20** No. 1 (1975) 33.

15) Badasarov, A. A., Berlizov, A. B., Vasin, N. L., Vertiporokh, A. N., Vinogradov,

V. P., Gorbunov, E. P., Dnestrovskij, Yu. N., Esipchuk, Yu. V., Zaveryaev, V. S., Izvozchikov, A. B., Kislov, A. Ya., Luk'yanov, S. Yu., Lysenko, S. E., Maksimov, Yu. S., Notkin, G. E., Pereverzev, G. V., Razumova, K. A., Strelkov, V. S. and Shcheglov, D. A.: *Studies on Ohmic Heating in T-10*, Proc. 7th Int. Conf. Plasma Phys. and Contr. Nuclear Fusion Res. (Innsbruck, Austria 1978) Vol. **I**, IAEA-CN-37/A-2, 35.

16) Zaveryaev, V. S., Izvozchikov, A. B., Lysenko, S. E. and Petrov, M. P.: *Ion Heating in the T-10 Tokamak*, Sov. J. Plasma Phys. **4** No. 6 (1978) 671.

17) Hasted, J. B.: Proc. Roy. Soc. (London) **A227** (1955) 466.

18) Artsimovich, L. A.: *Tokamak Devices*, Nuclear Fusion **12** (1972) 215.

19) Toi, K. and Takeda, T.: *Analysis of Tokamak-Plasma Steady State by Non-Linear Programming*, Nuclear Fusion **14** No. 4 (1974) 577.

20) Nelder, J. A. and Mead, R.: Computer J. **7** (1965) 308.

21) Petrov, M. P.: *Experimental Observation of Trapped Particles in Tokamak Devices*, Sov. Phys. Tech. Phys. **13** No. 5 (1968) 708.

22) Petrov, M. P.: *The Effect of Corrugation of the Longitudinal Magnetic Field on the Ion Component of Plasma in Tokamaks*, Proc. Int. Conf. on Plasma Phys. and Contr. Nuclear Fusion Res. (Tokyo, Japan 1974) IAEA-CN-33/A2-2, 43.

23) Wagner, F. and Mayer, H. M.: *Investigation of the Fast Neutral Particle Corona surrounding the Pulsator Plasma*, Proc. 8th Eur. Conf. Contr. Fusion and Plasma Phys. (Prague, Czechoslovakia 1977) Vol. **I**, 24.

24) Düchs, D. F., Post, D. E. and Rutherford, P. H.: *A Computer Model of Radial Transport in Tokamaks*, Nuclear Fusion **17** No. 3 (1977) 565.

25) Dnestrovskij, Yu. N., Lysenko, S. E. and Kislyakov, A. I.: *Recombination-Induced Neutral-Particle Flux in Tokamaks*, Nuclear Fusion **19** No. 3 (1979) 293.

26) Kitamura, A., Takahashi, K. and Yano, S.: Report of Japan Atomic Energy Research Institute, JAERI-M 5275 (1973).

(Received December 3, 1979)

Appendix A. Stray magnetic field around TRIAM-1

If there is stray magnetic field B_s between the stripping cell and the ceratrons, the orbit of the stripped ion is disturbed, i.e. the orbit is curved in the direction perpendicular to both the normal orbit and the stray magnetic field. For example in case of $B_s = 2$ G, the ion of 0.7 keV leaving the center of the entrance of the analyzer is shifted 1.2 mm from the center of the 7th exit. Since the diameter of the entrance of the ceratron (EMS-6081 B) is 11 mm, the stray field at the region should be suppressed within 2 G.

The stray magnetic field around TRIAM-1 was measured on the equatorial plane during the discharge. The results are shown in Fig. A-1. The radial magnetic field B_R does not change even if the plasma current changes. The vertical field B_Z in case of the plasma current $I_p = 30$ kA is nearly equal to the sum of the vertical field B_z in case of $I_p = 0$ kA and the calculated vertical field B_z made by only plasma

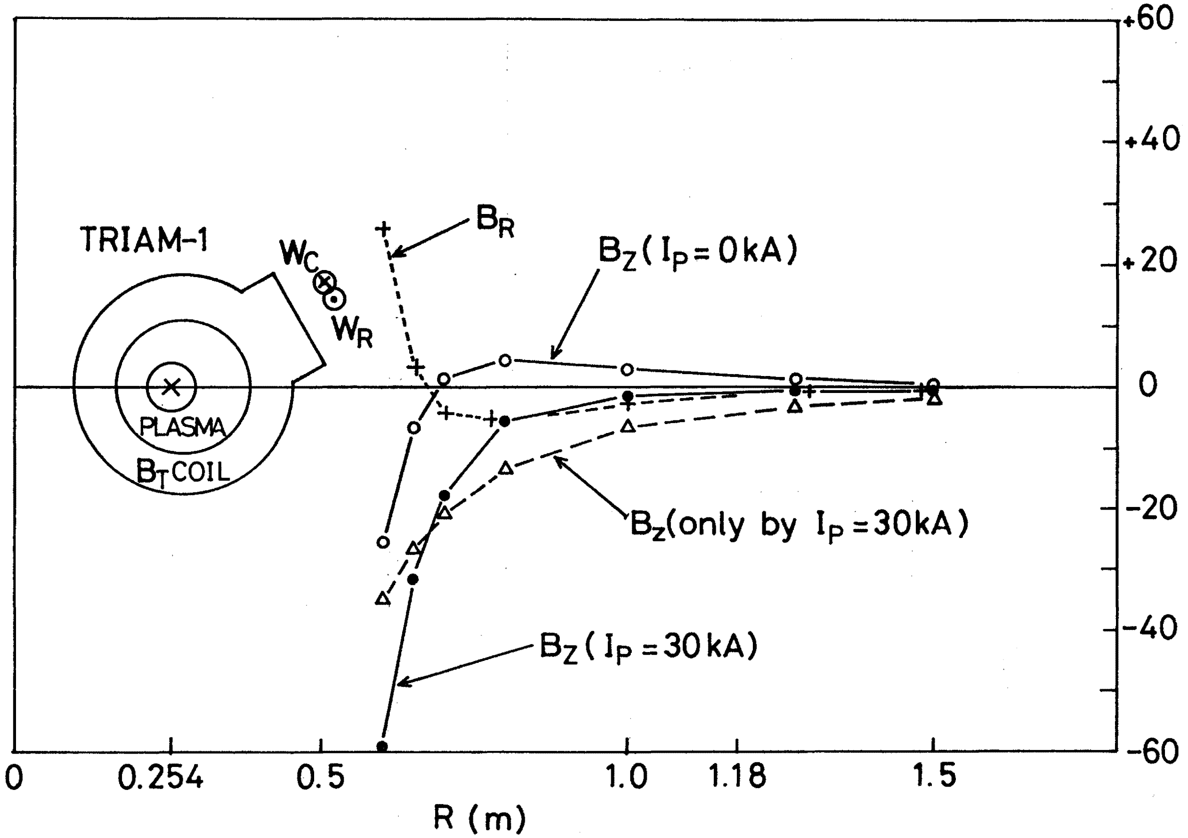

Fig. A-1 The distribution of the stray magnetic field around TRIAM-1.

R: radial distance from the main axis, W_C: connecting wire of B_T coil,
W_R: return winding of B_T coil, B_R: radial stray field,
B_Z: vertical stray field, B_z (only by I_p=30 kA) is the calculated value.

current (I_p=30 kA). The magnetic field B_R and B_z (I_p=0 kA) are explained to be the stray field by the current of the connecting wire W_c and the return winding W_R of the toroidal magnetic field coils concerning both the direction and the magnitude. The stray magnetic field B_s is smaller than 2 G at the place $R \geqq 1.18$ m (R=1.18 m is the radial distance of the center of the stripping cell from the symmetric axis of TRIAM-1).

Appendix B. Conversion factor in the stripping cell

The conversion factor η of $\underline{H}$ (emitted from a plasma) in the stripping cell filled with hydrogen gas is estimated as[26]

$$\eta = \frac{\sigma_{cs}}{\sigma_{cs}+\sigma_{cx}} [1-e^{-\pi(\sigma_{cs}+\sigma_{cx})}] \tag{B-1}$$

where σ_{cs} is the cross section of the charge stripping ($\underline{H}+H_2 \rightarrow \underline{H}^+ + H_2 + e^-$), σ_{cx} is that of the charge exchange ($\underline{H}^+ + H_2 \rightarrow \underline{H} + H_2^+$), and $\pi = 6.61 \times 10^{16}\, pl$ (p is the pressure of H_2 in Torr and l is the length of the stripping cell in cm). The cross sections of all are in cm^2. In our case ($p = 4\times10^{-4}$ Torr and l = 20 cm) the conversion factor is approximately expressed by $\eta \approx \pi\sigma_{cs} (\propto pl)$ within the 10 % error.

Figure B-1 shows the conversion factor η obtained for cases of $pl = 1.25\times10^{-2}$Torr•cm and $pl = 5\times10^{-2}$Torr•cm in DITE[6]. From this figure, we can obtain the conversion factor η in TRIAM-1 by the proportional estimation with respect to pl-value ($pl = 0.8\times10^{-2}$Torr•cm). The results are listed up in Table B-1.

Appendix C. Experimental error of the ion-temperature determination

We estimate the confidence interval of the ion temperature T_i as follows: If we define the variables x and y as

$$x \equiv E\,, \tag{C-1}$$

$$y \equiv \ln F\,, \tag{C-2}$$

the regression line of y on x is

$$y-\bar{y} = \beta_{yx}(x-\bar{x})\,, \tag{C-3}$$

where $\bar{x}$ and $\bar{y}$ are the arithmetic means of data points x and y, respectively. The regression coefficient of sample is

$$\beta_{yx} \equiv -1/T_i = r_{xy}s_y/s_x\,, \tag{C-4}$$

where r_{xy} is correlation coefficient of sample and is expressed as

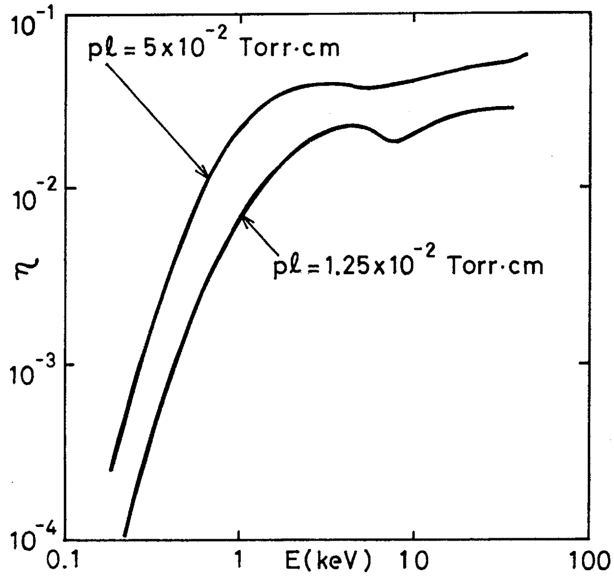

Fig. B-1 The conversion factor for $\underline{H}$ incident on the H_2 stripping cell in DITE[6].

Table B-1. The conversion factor η of $\underline{H}$ in the stripping cell of our device filled with hydrogen as a function of the energy E in case $p=4\times10^{-4}$ Torr for hydrogen.

E (keV)	η	E (keV)	η
0.2	4.9×10^{-5}	1.8	8.8
0.3	2.1×10^{-4}	2.0	9.9
0.4	5.5	2.5	1.2×10^{-2}
0.5	9.8	3.0	1.3
0.6	1.5×10^{-3}	4.0	1.4
0.7	2.2	5.0	1.4
0.8	2.9	6.0	1.3
0.9	3.5	7.0	1.2
1.0	4.2	8.0	1.2
1.2	5.5	9.0	1.2
1.4	6.9	10.0	1.3
1.6	7.9		

$r_{xy}=C_{xy}/s_x s_y$ (C_{xy}: covariance, s_x and s_y standard deviation).
The variable z obtained by z-transformation of r_{xy} follows as normal distribution $N(m, 1/n-3))$:

$$z = 0.5 \ln (1+r_{xy})/(1-r_{xy}) , \tag{C-5}$$
$$m = 0.5 \ln (1+\rho)/(1-\rho) , \tag{C-6}$$

where ρ: correlation coefficient of population,
n: the number of data points.
The confidence interval of m with confidence coefficient 90 % is

$$|z-m| < 1.64/\sqrt{n-3} , \tag{C-7}$$
$$m_1 \equiv z-1.64/\sqrt{n-3} < m < z+1.64/\sqrt{n-3} \equiv m_2 , \tag{C-8}$$
$$\rho_1 \equiv (e^{2m_1}-1)/(e^{2m_1}+1) < \rho < (e^{2m_2}-1)/(e^{2m_2}+1) \equiv \rho_2 . \tag{C-9}$$

Consequently the regression coefficient of population B is

$$B_1 \equiv \rho_1 s_y/s_x < B < \rho_2 s_y/s_x \equiv B_2 , \tag{C-10}$$
$$T_L \equiv -s_x/\rho_1 s_y < T_i \equiv -s_x/r_{xy} s_y < -s_x/\rho_2 s_y \equiv T_H , \tag{C-11}$$
$$T_L \equiv r_{xy} T_i/\rho_1 < T_i < r_{xy} T_i/\rho_2 \equiv T_H . \tag{C-12}$$

For example we estimate the experimental error of the bulk ion temperature from the data shown in Fig. 8(a),

$\bar{x} = 524$, $\bar{y} = -0.483$,
$s_x = 806$, $s_y = 2.43$, $C_{xy} = -1537$,
$r_{xy} = -0.785$, $\beta_{yx} = -2.36$, $z = -1.06$,
$m_1 = -1.35$, $m_2 = -0.886$,
$\rho_1 = -0.874$, $\rho_2 = -0.709$,
$T_L = 144 < T_i = 160 < T_H = 177$,
$T_i = 160^{+17}_{-16}$.